Cell cycle checkpoint activity in the malaria parasite *Plasmodium falciparum*

Monique K. Johnson[1], Juliana Naldoni[1], Catherine J. Merrick[1*]

[1] Department of Pathology, University of Cambridge, Tennis Court Road, Cambridge, CB2 1QP, UK.

* Address correspondence to:

Department of Pathology, Cambridge University, Tennis Court Road, Cambridge, CB2 1QP, UK

Tel: (+44) 1223 333330

CJM: Email: cjm48@cam.ac.uk

ABSTRACT

Plasmodium spp. have different modes of cell division from most eukaryotes. Little is known about how these are controlled and cell-cycle checkpoints are particularly poorly characterised. However, parasites can arrest their cell cycle when treated with the frontline antimalarial drug artemisinin, and artemisinin-resistant parasites can modulate their cell-cycle progression, so it is very important to understand these aspects of *Plasmodium* biology. Here, we show that *P. falciparum* displays hallmarks of an intra-S-phase checkpoint when exposed to DNA damage, including acute reduction of DNA replication and phosphorylation of a putative damage-marker histone. Compounds that inhibit human checkpoint kinases can inhibit this arrest of DNA replication, and synergise with DNA damage in parasite killing. This suggests the existence of checkpoint kinase activity in *P. falciparum*, yet these kinases have no clear homologues in *Plasmodium* genomes. We hypothesise that phosphatidylinositol 3-kinase – an essential lipid kinase – may moonlight in this role: it is the closest homologue to a checkpoint kinase and is reportedly up-regulated in artemisinin-resistant parasites. Finally, we show that the cryptic checkpoint-kinase activity may also regulate the ring-stage survival phenotype after artemisinin damage, which resembles a G1/S checkpoint. Hence we suggest that checkpoint kinase inhibitors are candidates for synergy with artemisinin.

AUTHOR SUMMARY

Malaria parasites cause illness by infecting human red blood cells, wherein they replicate to produce many new parasites within ~1-3 days. This is unusual because most cells (such as human cells) replicate simply by copying their genome and splitting in half – which is called binary fission – but malaria parasites make ~20 genome copies and then partition them simultaneously into 20 new cells – which is called schizogony. Here we studied how these parasites control schizogony. In particular, do they have 'checkpoints': the ability to pause the cell cycle for repair if the genome is damaged? We found that DNA damage during active replication *did* cause hallmarks of a checkpoint, despite the fact that all the key proteins that enforce this in other cells are absent in malaria parasites. Furthermore, this checkpoint activity may be involved in the response to the antimalarial drug artemisinin: a response that parasites make by pausing their cycle before active replication begins. This could be important because it implies that inhibiting the checkpoint could exacerbate parasite killing by artemisinin-based drugs, similar to the way that some cancer therapies work by damaging DNA and also preventing the cancer cells from repairing it.

KEYWORDS

Malaria, *Plasmodium,* cell cycle, checkpoint, PI3K

INTRODUCTION

Plasmodium falciparum is the most important cause of human malaria, giving rise to over half a million deaths and hundreds of millions of clinical cases per year [1]. Besides being a major human pathogen, this is also a highly unusual, early-diverging protozoan organism, with distinctive features of cell and molecular biology. One of these is a non-canonical cell cycle. Instead of dividing by binary fission, as in most model organisms, *Plasmodium* parasites divide primarily by schizogony. After invading a host erythrocyte, they execute multiple, asynchronous rounds of genome replication and nuclear division, generating a syncytium of nuclei within the same cytoplasm. This is followed by a mass cytokinesis event, partitioning as many as 20-30 nuclei and organelles into individual merozoites.

50 The complex events of schizogony are now being dissected in considerable molecular and
51 cellular detail [2-5] but fundamental questions remain about how the process is regulated.
52 Schizogony is not easily mapped onto the well-characterised cell cycle phases of G1, S, G2 and M.
53 After invading a new host cell, the parasite undergoes a pre-replicative growth phase broadly
54 analogous to G1. The haploid genome is then repeatedly replicated in a continuous S-phase without
55 once-and-only-once regulation, generating many new haploid nuclei. Different nuclei cease to
56 replicate at different times, and divide at different times, so there is no well-defined G2 and no
57 single M-phase [3].

58 *Plasmodium* replication is not controlled by conventional waves of cyclin and cyclin-
59 dependent kinase activity [6]. Nor is it apparently governed by conventional cell cycle checkpoints,
60 which usually operate at the G1/S transition, within S-phase, and at G2/M. Respectively, these
61 checkpoints delay the start of S-phase, arrest replication if DNA damage or replication stress is
62 detected, and prevent mitosis if a genome is incompletely replicated [7]. The *Plasmodium* genus,
63 however, encodes no clear homologs of the checkpoint kinases conserved from yeast to humans:
64 Mec1 and Rad53 in *S. cerevisiae* and their homologs ATM/ATR and Chk1/Chk2 in mammalian cells
65 [6]. Some parasites in the apicomplexan phylum, including *Toxoplasma*, do retain homologs of the
66 'master regulators' Mec1/ATM/ATR, which are phosphoinositide-3-kinase-like kinases (PIKKs), but
67 *Plasmodium* does not [8].

68 Nevertheless, eukaryotic cells generally do pause their cell cycles to ensure effective DNA
69 repair and faithful DNA replication – not only in metazoans, which must guard against cancer, but
70 also in protozoans. *Plasmodium* encodes most of the known DNA repair pathways [6, 9] and
71 generates relatively low rates of SNPs, indels and translocations during normal replication [10], so it
72 seems unlikely that it is entirely without checkpoints.

73 There is some evidence for a G1/S-like checkpoint: pre-replicative rings can undergo
74 'temporary growth arrest (TGA)' [11] in response to nutritional, temperature or antimalarial-drug

75 stresses. TGA is particularly important under stress caused by the antimalarial drug artemisinin,
76 because it can contribute to treatment failure. However, there is no molecular evidence as-yet that
77 conventional checkpoint effectors are involved. A G1/S checkpoint usually involves the cyclin/CDK
78 complexes that drive S-phase entry, influenced positively by growth factors or negatively by damage
79 responsive kinases like PIKKs. TGA, by contrast, is defined only as a 'non-specific stress-response
80 survival mechanism' [11]: induced by multiple stresses, possibly via multiple molecular pathways.

81 An intra-S-phase checkpoint, meanwhile, should arrest S-phase specifically after DNA
82 damage or replication stress. After DNA damage, the transcriptional cascade that drives the
83 *Plasmodium* cell cycle can slow down, with DNA repair proteins and chromatin modifications being
84 upregulated [12], but the signals and transducers for this potential checkpoint are unknown.
85 *Plasmodium* generally lacks validated markers for DNA damage and for direct responses to it.

86 Finally, a G2/M checkpoint may be entirely absent because some *P. falciparum* mutants
87 perform grossly aberrant genome segregation but still undergo cytokinesis [13]. In fact, even in non-
88 mutants, certain phases of the lifecycle produce a high rate of zoids – particularly the rapid process
89 of gametogenesis inside the mosquito, when male cells produce and segregate eight new genomes
90 into mature, motile gametes in less than 15 minutes. Here, cytokinesis proceeds even if genome
91 replication fails entirely [14, 15].

92 Here, we set out to investigate checkpoint responses to DNA damage in *Plasmodium,* using
93 newly developed molecular and cellular tools. We show that the hallmarks of an S-phase checkpoint
94 do occur in *P. falciparum*, despite the apparent absence of PIKKs.

95 **RESULTS**

96 <u>Evidence for DNA-damage-responsive checkpoint activity in *P. falciparum*</u>

97 We used two complementary tools to investigate the response to DNA damage during S-phase in *P.*
98 *falciparum*, focussing at the levels of DNA and protein. Firstly, we labelled nascent DNA in

99 replicating parasites with a quantifiable modified nucleotide. This tested whether DNA replication
100 could be acutely arrested after damage: a hallmark of the intra-S-phase checkpoint [16, 17].
101 Secondly, we measured phosphorylation of histone H2A, which was recently identified as being
102 analogous to histone H2AX phosphorylation in mammalian cells [18]. Canonically, H2AX is
103 phosphorylated by ATM/ATR at chromatin sites of DNA damage [19, 20]. H2AX is absent in
104 *Plasmodium*, as are ATM and ATR, but the non-variant histone H2A can nevertheless be
105 phosphorylated by unidentified kinase(s) [18]. Importantly, this indicates an *in trans*, kinase-driven,
106 genuinely 'checkpoint-like' response.

107 To induce DNA damage, we used the well-characterised alkylating agent methyl methane
108 sulphonate (MMS), which alkylates DNA bases, particularly guanine and adenine [21]. In mammalian
109 cells, it induces an intra-S-phase checkpoint [16]. In *P. falciparum* parasites, it leads to DNA
110 breakage, as measured by comet assays [22] and concomitantly delays the cell cycle [12], but its
111 effect as a checkpoint inducer has not been explicitly addressed. In the *P. falciparum* 3D7 strain,
112 MMS had a 48h IC_{50} of ~96µM (Fig S1A). Having established this, we performed highly acute assays
113 over just 1-2h, using 10x or 20x IC_{50}, to minimise non-specific or secondary effects. We confirmed
114 that parasites could substantially recover from this level of MMS exposure within one cell cycle,
115 although their maturation was delayed, as reported previously [12], and there was also a reduction
116 in merozoite numbers in mature schizonts (Fig S2).

117 DNA replication was acutely reduced in the 30 minutes following a 30-minute exposure to
118 MMS at 10x or 20x IC_{50}. Some reduction occurred throughout S-phase (~28-36 hours post invasion,
119 hpi) but it was most pronounced when DNA was damaged in early trophozoites (~32hpi) (Fig 1A).
120 Within a similar timeframe, histone H2A phosphorylation was moderately elevated (Fig 1B). We
121 recently reported that several DNA damaging agents, including MMS, could cause H2A
122 phosphorylation [23], but that the upregulation was transient and modest – usually less than 2-fold
123 over background levels – making it difficult to measure consistently. This was equally true when

124 MMS was used to induce H2A phosphorylation here (Fig 1B). (Previously published work measured
125 H2A phosphorylation in pre-replicative rings exposed to ionising radiation [18], whereas we
126 measured it in actively replicating trophozoites.) Therefore, we chose the replication-reduction
127 assay as a more robust readout for checkpoint activity in subsequent experiments.

128 Possible mediators of checkpoint activity in *P. falciparum*

129 When the intra-S-phase checkpoint is triggered in other eukaryotes, both histone phosphorylation
130 and arrest of DNA replication are transduced through PIKKs [17, 19]. Since Figure 1 shows that these
131 phenotypes also appear in *P. falciparum,* a transducing kinase activity should be present. However,
132 there is no obvious candidate in the *P. falciparum* genome [8]. The closest PIKK homologues in any
133 *Plasmodium* genome are the lipid kinases PI3K and PI4K (Fig S3), whereas other apicomplexans such
134 as *Toxoplasma* encode additional kinases homologous to PIKKs [8]. Notably, the closest *Plasmodium*
135 homologue, PI3K, has been reported to be overexpressed in artemisinin resistant parasites [24],
136 which can alter their cell cycle dynamics. Accordingly, we hypothesised that PI3K might act as a
137 checkpoint kinase in *Plasmodium.*

138 *Pf*PI3K is the only phosphoinositide 3-kinase of the six phosphoinositide kinases in
139 *Plasmodium* [25]: it is a well-validated, essential lipid kinase [26] with roles in nutrient uptake and
140 vesicle trafficking [27, 28]. We hypothesised that it might also 'moonlight' as a protein kinase, which
141 would not be unprecedented, as other PI3Ks can to act on proteins as well as lipids. For example,
142 humans encode a large family of PI3Ks, and the type-1 PI3Ks can phosphorylate protein substrates
143 such as cytokine receptors, as well as auto-phosphorylating themselves [29, 30]. The sole
144 *Plasmodium* enzyme is a type-3 PI3K, and thus far these are proven only to phosphorylate lipids [26].

145 If our hypothesis was correct, then *Pf*PI3K should have some activity within the nucleus,
146 phosphorylating substrates such as histone H2A. To track the protein *in cellulo,* we raised peptide
147 antibodies (modelling for peptide selection is shown in Fig S4A), which detected a protein of the
148 correct 256kDa size (Fig 2A). In immunofluorescence, *Pf*PI3K appeared dispersed and cytoplasmic

149 (Fig 2B, Fig S4B), consistent with a previous publication that suggested a location in transport
150 vesicles [28]. We did not detect any substantial re-location to the nucleus upon DNA damage (Fig
151 2C). However, we recently showed that the ATM and ATR homologues in *Toxoplasma* are likewise
152 dispersed throughout the cell and do not detectably relocate to the nucleus after DNA damage, but
153 they are nevertheless able to mediate checkpoint phenotypes such as histone phosphorylation [8].

154 Further experiments were precluded because the *Pf*PI3K enzyme is essential and cannot be
155 knocked out (probably due to its unique lipid kinase activity): several attempts were made to 3' tag
156 the gene for conditional knockdown instead, but these failed, probably because the enzyme's active
157 site is encoded at the extreme 3' end and may become mis-folded after 3' tagging. The large size of
158 the *PfPI3K* gene (6.6kb) precluded overexpression, dominant-negative overexpression or
159 recombinant protein production for enzyme-activity assays. Attempts were also made to
160 immunoprecipitate the native protein with its potential substrates, but only a single *Pf*PI3K peptide
161 was detected across several immunoprecipitation attempts – probably because the kinase is lowly
162 expressed, very large, and unstable *in vitro*. Thus, the putative PIKK-like activity of *Pf*PI3K remained
163 neither evidenced nor disproved.

164

165 <u>The mediator of DNA-damage checkpoint responses in *Plasmodium* is sensitive to PIKK inhibitors</u>

166 Despite the lack of conclusive evidence for *Pf*PI3K as a checkpoint kinase, a divergent PIKK-like
167 kinase may nevertheless exist in *P. falciparum*, and hence we attempted to inhibit it with PIKK
168 inhibitors. We chose two compounds that had validated specificity for human ATM and ATR
169 respectively, KU-55933 and VE-821 [31, 32]. If an ATM-like and/or ATR-like activity existed in *P.*
170 *falciparum*, either within *Pf*PI3K or in another protein, these compounds might specifically inhibit it.
171 We first determined their 48h IC_{50} values on *P. falciparum* (3D7 strain): KU-55933 had an IC_{50} in the
172 micromolar range and VE-821, in the nanomolar range (Fig 3A, Fig S1B).

173 Both inhibitors clearly synergised with MMS in a 48h isobologram analysis, particularly
174 strongly in the case of VE-821, suggesting activity within the same pathway (Fig 3B). Control
175 compounds that kill parasites but are not known to cause DNA damage – the antibiotics blasticidin
176 and geneticin – did not synergise with MMS (Fig S5). Furthermore, when parasites were exposed to
177 high-dose MMS (10x IC_{50}, as in Figure 1) simultaneously with KU-55933 or VE-821, the inhibitors
178 ablated the acute reduction in DNA replication caused by MMS, whereas co-exposure to the control
179 antibiotic geneticin did not (Fig 3C). In this short 1h assay, we used the PIKK inhibitors at only their
180 48h IC_{50} levels, to minimise any negative effects from the inhibitors alone. Indeed, within the
181 timeframe of the assay the inhibitors alone did not significantly affect DNA replication (Fig 3C).
182 Overall, these data strongly supported the existence of a cryptic PIKK activity, responsible for a
183 genuine intra-S-phase checkpoint via *in trans* kinase activity.

184

185 The antimalarial drug dihydroartemisinin induces DNA replication arrest in *P. falciparum*

186 MMS is a useful, well-characterised DNA-damaging agent, but it is not an antimalarial drug. We
187 were particularly interested in the potential DNA-damaging activity of antimalarial drugs, because if
188 parasites do make checkpoint responses to such drugs, then their antimalarial activity might be
189 potentiated by inhibiting checkpoint kinases. Artemisinin is such a drug: it has non-specific alkylating
190 activity that may affect both proteins and DNA [33, 34]. There are similarities between the
191 parasite's response to dihydroartemisinin (DHA, the active metabolite of artemisinin) and MMS in
192 terms of DNA breakage [33, 35], delay in the parasite's transcriptional cascade, and upregulation of
193 DNA repair genes [12].

194 Using the replication-reduction assay (Fig 4A), we saw that DHA caused an acute reduction in
195 nascent DNA replication, similar to MMS. However, unlike MMS, this was not ablated by the PIKK
196 inhibitors KU-55933 and VE-821. Consistent with this difference, the inhibitors did not synergise
197 with DHA in isobologram analysis (Fig 4B). This suggested that although both DHA and MMS may

198 damage DNA, they differ in either the type of damage or the cellular response thereto in terms of an
199 intra-S-phase checkpoint.

200

201 Ring-stage survival after artemisinin damage is affected by PIKK inhibitors

202 Cell-cycle checkpoint activity in *P. falciparum* may not be limited to an intra-S-phase checkpoint:
203 most eukaryotic cells also operate a G1/S checkpoint, delaying S-phase entry if cells are damaged,
204 starved or stressed. This may be analogous to the 'TGA' arrest or 'dormancy' that occurs in ring-
205 stage parasites after various stressors, including artemisinin treatment [11]. We therefore set out to
206 establish whether ring-stage dormancy induced by DHA actually represents a classical, PIKK-
207 mediated G1/S checkpoint.

208 We conducted the ring-stage survival assay (RSA) on parasites treated with DHA in the
209 presence or absence of PIKK inhibitors. In this assay, pre-replicative early-ring-stage parasites are
210 damaged with a pulse of DHA: most of them die, but some successfully arrest and thence survive.
211 The more parasites are able to do this, the higher the subsequent recovery of viable parasites. We
212 reasoned that if successful arrest is due to PIKK-mediated checkpoint activity, then PIKK inhibitors
213 should reduce ring-stage survival. These experiments were conducted in the 3D7 strain and also in
214 the Cambodian strain MRA-1252. MRA-1252 was derived from a naturally-arising DHA-resistant
215 strain, which was genetically reverted back to a sensitive phenotype by reverting the resistance
216 mutation in the gene encoding Kelch13 [36]. Its genetic background is otherwise that of a S.E. Asian
217 DHA-resistant line. Both 3D7 and MRA-1252 are highly sensitive to artemisinin, so we used the
218 'extended recovery ring-stage survival assay' (eRRSA), which detects recovered parasites very
219 sensitively after 72h via quantitative PCR [37].

220 Figure 5A shows that PIKK inhibitors, particularly KU-55933, did indeed exacerbate the killing
221 of ring-stage parasites by DHA. Differences were only subtle and parallel assays using the more

222 common but less sensitive flow cytometric assessment of live/dead cells to read the RSA likewise
223 showed only marginal differences (Fig S6). However, in both 3D7 and MRA-1252, triplicate eRRSAs
224 showed that survival trended downwards when DHA was combined with either inhibitor. Neither
225 condition (DHA + VE-821 or DHA + KU-55933) reached statistical significance versus survival after
226 DHA alone, but the p-values versus control were < 0.0001 rather than 0.001. As above, we
227 minimised any negative effects of the inhibitors themselves by using them at a low level – only half
228 of the 48h IC_{50}. We confirmed that this exposure alone for 6h did not affect parasite survival after
229 72h (Fig 5B).

230 These RSAs did not show conclusively that 'TGA' after artemisinin damage represents a true
231 G1/S checkpoint. However, they did suggest that such a checkpoint, mediated by a cryptic PIKK, may
232 contribute to ring-stage survival. Hence, the cryptic PIKK must be active throughout the cell cycle,
233 not only in actively replicating trophozoites.

234 When the same assay was conducted on DHA-resistant parasites (the parent strain of MRA-
235 1252, called MRA-1240) the result differed. As expected, DHA survival was much better in MRA-
236 1240, and PIKK inhibitors had no negative effect on this survival (Fig 5C). If anything, there was a
237 trend towards better growth and better DHA survival when MRA-1240 was exposed to PIKK
238 inhibitors (Fig 5D). Hence, when a Kelch13 mutation was present, conferring DHA resistance, any
239 contribution of checkpoint activity to parasite survival was apparently ablated.

240

241 <u>Artemisinin-resistant parasites are cross-resistant to MMS and VE-821, but not to KU-55933</u>

242 We hypothesised that artemisinin-resistant (Kelch13 mutant) parasites might not require 'G1/S'
243 checkpoint activity to survive DHA damage because they are more efficient at DNA repair. Several
244 mutations in DNA repair genes have been identified in resistant strains [34], although the pathway(s)
245 leading to improved DNA repair remain to be fully characterised. We checked whether the DHA-
246 resistant line MRA-1240 was cross-resistant to MMS, and its IC_{50} was indeed significantly higher than

247 that of the matched sensitive line MRA-1252 (and also higher than that of 3D7) (Fig 5E, left panel; Fig
248 S1C). Since the point mutation in Kelch13 is the only difference between the two Cambodian MRA
249 lines, a genetic background of enhanced DNA repair cannot fully account for this.

250 One other explanation for an improved DNA repair capacity in resistant parasites could be
251 that they have hyper-active checkpoint activity (possibly due to Kelch13-associated over-expression
252 of PI3K [24]) and that this stimulates hyperactive DNA repair. This explanation *would* be consistent
253 with MRA-1240 (Kelch13-mutant) and MRA-1252 (revertant) having different sensitivities to MMS.
254 If so, the Kelch13 mutant state would also be expected to correlate with reduced sensitivity to PIKK
255 inhibitors. Indeed, MRA-1240 was much less sensitive than MRA-1252 to the VE-821 inhibitor (Fig
256 5E, middle panel; Fig S1C) – so much so that it was difficult to measure a consistent IC_{50} via MSF
257 assay. Curiously, however, the same line was not less sensitive to KU-55933 (Fig 5E, right panel; Fig
258 S1C). This was the first instance in which VE-821 and KU-55933 had shown a clear difference in their
259 effects on *P. falciparum*. It may suggest that more than one checkpoint protein is required, at least
260 in the MRA-1240/1252 genetic background, and that one of the inhibitors has a broader inhibitory
261 spectrum than the other. For example, *Pf*PI3K may indeed moonlights as a checkpoint kinase, but
262 *Pf*PI4K may also be required for certain checkpoint pathways. These speculations urgently require
263 conditional genetic manipulation of these large, essential kinase-encoding genes.

264 **DISCUSSION**

265 This work provides the first evidence that *Plasmodium* parasites during blood-stage schizogony can
266 enforce an intra-S-phase checkpoint. The checkpoint is evidenced by an acute reduction in the rate
267 of DNA replication and the phosphorylation of histone H2A in a position analogous to the canonical
268 DNA damage marker H2AX. *P. falciparum* was previously shown to slow its cell-cycle progression
269 after DNA damage [12] but it was not clear if this occurred through cell-cycle checkpoint activity
270 (partly because the *Plasmodium* system lacked validated DNA damage markers, signals or
271 transducers thereof). Markers still remain limited – there are, for example, no cyclin markers for

272 cell-cycle phases, and the H2A phosphorylation that has been reported as a DNA damage marker in
273 ring stages [18] is not, in our hands, a very strong marker in trophozoite stages (possibly because
274 background phosphorylation levels are higher in actively-replicating parasites). However, the ability
275 to measure nascent DNA replication in *Plasmodium* [38] does now allow intra-S-phase checkpoints
276 to be measured. Thus we showed that DNA replication was acutely arrested by two distinct
277 alkylating agents, MMS and the antimalarial drug DHA.

278 The transducer(s) of checkpoint activity in *Plasmodium* remain cryptic. *Plasmodium* spp.
279 lack identifiable homologues of PIKK kinases, in contrast to many apicomplexans including *T. gondii*
280 [8]. Nevertheless, such activity is apparently present, because the reduction in replication caused by
281 MMS was ablated by well-validated inhibitors of human PIKKs. Hence it must be induced *in trans* by
282 a genuine kinase-mediated signalling cascade (also consistent with H2A phosphorylation), rather
283 than occurring simply because alkylated bases physically block the movement of replisomes.
284 Interestingly, DHA differed from MMS in this respect: it also affected DNA replication, but PIKK
285 inhibitors did not ameliorate this. Possibly the acute effect of DHA – which is a larger molecule than
286 MMS – *is* primarily to block replisomes via bulky DNA adducts (a documented effect of alkylating
287 agents in human cells [16]), and these cannot be bypassed whether a checkpoint kinase is active or
288 not, while a lesser role is played by *in trans* checkpoint signalling after DHA damage.

289 Other, more complex, explanations for the difference in response to MMS versus DHA are
290 also possible. For example, slow DNA replication can, in general, stimulate compensatory activation
291 of extra replication origins [39], but when DNA damage is sensed, checkpoint kinases act to suppress
292 such origin firing *in trans* [16]. If checkpoint kinases are inhibited, then extra origins may fire
293 regardless, hence MMS-damaged cells may keep replicating, eventually encountering more damage,
294 so genome replication ultimately fails to complete. This would explain how MMS and PIKK inhibitors
295 ultimately synergise in cell killing. Perhaps the broader-spectrum damage that DHA causes to
296 proteins as well as DNA [33], and/or the oxidative stress that it generates [35] means that

297 compensatory origin firing does not happen, whether a checkpoint is activated or not. Hence PIKK
298 inhibitors would not synergise with DHA in cell killing. To evidence these rather complex
299 hypotheses, precision measurement of DNA replication dynamics at single-molecule resolution after
300 different types of damage will be needed. This has been achieved in human cells [16], and is now in
301 development for *Plasmodium*.

302 Turning to the possibility of a pre-replicative G1/S checkpoint, the evidence for this being
303 mediated by a PIKK-like kinase is not yet conclusive, but nevertheless tantalising. In the RSA, which
304 measures DHA killing of pre-replicative rings, PIKK inhibitors exacerbated parasite killing. This trend
305 was consistent (albeit not statistically significant) in triplicate assays across two genetically-distinct
306 DHA-sensitive strains, 3D7 and MRA-1252. Checkpoint kinase activity may help to protect ring-stage
307 cells, perhaps by detecting DNA damage, stimulating repair, and preventing S-phase entry until
308 repair is complete. By contrast, a DHA-resistant strain showed no effect of PIKK inhibitors. This may
309 be because it can already suppress DHA activation in early rings and thus protect itself from DNA
310 damage; or alternatively, it may still sustain some damage, but be rescued by hyperactive DNA
311 repair [34].

312 If there is indeed hyperactive DNA repair, it cannot be conferred by a DHA-resistant genetic
313 background because the matched strain MRA-1252 was not cross-resistant to MMS, whereas MRA-
314 1240 was. However, it could be because the Kelch13 mutation, uniquely present in MRA-1240,
315 confers hyper-checkpoint activity, thus stimulating hyperactive DNA repair. In any case, these data
316 raise the intriguing possibility that artemisinin drugs could synergise with checkpoint inhibitors in
317 killing ring-stage parasites; the caveat being that this might only work well in sensitive, not resistant,
318 strains.

319 It is an attractive idea that *Pf*PI3K is the cryptic checkpoint kinase, particularly if Kelch13
320 mutant strains do contain more *Pf*PI3K [24]. However, we were not yet able to prove or disprove
321 this, owing to the difficulty of manipulating the large, essential *PfPI3K* gene. Broad-spectrum

322 inhibitors such as wortmannin were used in previous work [28], but these are slow-killing and unable
323 to separate lipid-kinase from putative protein-kinase activity. We used PIKK inhibitors instead,
324 hoping to isolate a putative protein kinase activity. The fact that our PIKK inhibitors did not
325 synergise with DHA in MSF assays, whereas specific inhibitors of distinct human PI3Ks (i.e. lipid
326 kinases) *have* been reported to do so [40], may suggest that this succeeded, and that VE-821 and
327 KU-55933 do target a distinct activity in *Plasmodium*. They may, of course, merely affect irrelevant
328 off-targets, but it is more likely that they genuinely inhibit a *Plasmodium* checkpoint kinase – which
329 may reside in *Pf*PI3K and/or *Pf*PI4K, or in another radically divergent protein.

330 In conclusion, we present new evidence for measurable cell-cycle checkpoint activity in
331 *Plasmodium*. We also raise the considerable challenge of unambiguously identifying its mediators in
332 this deeply-diverging eukaryote.

333 **METHODS**

334 **Parasite cultures**

335 *Plasmodium falciparum* cultures were grown in 2% or 4% haematocrit human erythrocytes
336 (Research Red Cells obtained from the NHS Blood & Transplant service), in RPMI 1640 (Sigma,
337 R4130) supplemented with 2.3 g/L sodium bicarbonate, 50 mg/L hypoxanthine (Sigma, H9377), 25
338 µg/L gentamicin (Melford Laboratories, G38000-1), 2.5 g/L Albumax II and 5% human serum.
339 Parasites were cultured under a 1% O_2/ 3% CO_2/ 96% N_2 gaseous atmosphere at 37 °C.

340 **Parasite strains**

341 Parasite strains used were: 3D7, 3D7 pTK, MRA-1240 and MRA-1252. 3D7 pTK carries a thymidine
342 kinase transgene to allow incorporation of bromodeoxyuridine (BrdU) for monitoring DNA
343 replication [38]. MRA-1240 and MRA-1252 are matched artemisinin-resistant and sensitive
344 Cambodian field lines, respectively [36], obtained through BEI Resources (NIAID, NIH). Parasites
345 were synchronised as in [41].

346 **BrdU Enzyme-linked immunosorbent assay (ELISA)**

347 ELISA was carried out as per [38]. In brief, tightly synchronised *P. falciparum* 3D7 pTK parasites were
348 collected at 4% parasitaemia and 4% haematocrit at 28 hpi, 32 hpi and 36 hpi. They were labelled
349 with BrdU (100 µM, Sigma) for 30 min and then collected for ELISA, or treated with MMS at 10 x IC_{50}
350 (960 µM) or 20 x IC_{50} (1,920 µM) for 30 min prior to BrdU labelling. In further experiments, parasites
351 at 30-32 hpi were exposed to either MMS alone (10x IC_{50}), MMS+VE-821 (1x IC_{50}), MMS+KU-55933
352 (1x IC_{50}), VE-821 alone, KU-55933 alone, DHA alone (10x IC_{50}), DHA+VE-821, DHA+KU-55933 or no
353 drugs, then processed as above.

354 **Immunofluorescence**

355 Air-dried thick blood smears were fixed with 4% paraformaldehyde in PBS for 10 min and
356 permeabilised for 10 min with 0.05% triton in PBS. Slides were then blocked for 1 h in 1% BSA/PBS.
357 The primary antibody was added in blocking buffer for 1 h under a coverslip. After 3x 5 min washes
358 in PBS, the secondary antibody was added to slides for 1 h. The slides were washed with PBS for 5
359 min, 120 µl of 2 µg/ml DAPI solution was added for 10 min and then the slides washed again with
360 PBS for 5 min. Coverslips were mounted on slides in Prolong® Diamond (Invitrogen) and allowed to
361 dry overnight at 4 °C. Images were acquired using a Nikon Eclipse Ti widefield microscope with a
362 Nikon objective lens (Plan APO, 100x/1.45 oil), and a Hamamatsu C11440, ORCA Flash 4.0 camera.
363 Images were processed using the NIS-Elements software and ImageJ (v.1.51w).

364 **Malaria SYBR Green-1 Fluorescence (MSF) assay**

365 MSF assays were conducted as in [42]. 100 µM chloroquine (Merck) was used as a control for
366 parasite death. Data were analysed and graphs plotted in GraphPad Prism.

367 **Isobolograms**

368 Parasites were prepared as for MSF assays. Isobologram design followed the procedure in [43].
369 Serial dilutions were planned so that the IC_{50}s of each drug would be in the second two-fold dilution
370 out of 6 total dilutions. IC_{50}s for each combination solution were calculated using sigmoidal best-fit

371 curves assigned in Graphpad Prism. Fractional inhibitory concentrations (FIC values) were calculated
372 in Excel [44] and isobolograms plotted in Graphpad Prism.

373 **Ring-stage Survival Assay (RSA)**

374 Parasite cultures at 8-10% schizonts were synchronised using percoll and Compound 2 as in [41],
375 then allowed to reinvade. Early ring-stage (0-3 hpi) parasites at 0.5% parasitaemia, 2% haematocrit
376 were exposed for 6 h to 700 nM DHA or 0.02% DMSO (vehicle control) under normal conditions,
377 before washing three times with incomplete media, resuspending in complete media and incubating
378 under the same conditions for a further 66 h. In addition to the DHA 700 nM pulse, VE-821 and KU-
379 55933 inhibitors were used at 0.5x IC_{50} with DHA, or by themselves, throughout the 6 h pulse period.
380 72 h after initial drug exposure, 20 µl was frozen for RT-PCR as per eRRSA protocol [37].

381 **qPCR-based RSA analysis**

382 qPCR amplification was used to quantify live parasites in the eRRSA [37]. The Phusion Blood Direct
383 PCR kit was used (ThermoFisher, cat # F547L), supplemented with 1x SYBR™ Green I (ThermoFisher)
384 and 50 nM Low ROX (ThermoFisher), according to the manufacturer's instructions. qPCR
385 amplification was measured using the fast mode of the ABI 7900HT, with a 20 s denaturation at 95
386 °C, followed by 35 cycles of 95 °C for 1 s, 62.3 °C for 30 s, and 65 °C for 15 s. Cycle threshold (Ct)
387 values were calculated; then the fold change was calculated by determining the mean difference in
388 Ct (ΔCt) for the three technical replicates between the untreated and DHA-treated samples by
389 applying the following equation: Fold change =2^(ΔCt of treated – ΔCt of untreated). This was -log
390 transformed and data were plotted in GraphPad Prism.

391 **Flow cytometry-based RSA analysis**

392 Flow cytometry wash buffer 'FC wash' (2% FBS (Gibco) in HBSS (calcium, magnesium, no phenol red,
393 Gibco) was prepared. The remaining 180 µl of each RSA assay, not harvested for eRRSA, was
394 centrifuged and packed cells were washed three times in 200 µL of FC wash, then resuspended in FC
395 wash to make a 10% haematocrit suspension. 25 µL of suspension from each assay (conducted in

396 technical triplicate) were mixed with 25 µL of 0.6X SYBR Green I (SYBR) with 1.5 nM MitoTracker
397 Deep Red FM (MT, Invitrogen) in FC wash. Compensation controls were prepared with suspension
398 from one DMSO-treated triplicate, labelled with either 0.6X SYBR, 1.5 nM MT, or FC wash alone.
399 Samples were incubated in the dark at 37°C for 30 min, then washed three times in 200 µL and
400 resuspended in 180 µL of FC wash.

401 10,000 events of SYBR positive cells were captured at a flow rate of 25 µL/min on an Attune NxT
402 Acoustic Focusing Cytometer (Invitrogen). SYBR and MT fluorescence were detected on the BL1 (488
403 nm excitation, 530/30 nm emission, 340 V) and RL1 (638 nm excitation, 670/14 nm emission, 510 V)
404 channels respectively. Debris and doublets were excluded by gating on a forward scatter area (FSC-
405 A) versus side scatter height (SSC-H) plot and forward scatter area (FSC-A) versus forward scatter
406 height (FSC-H). SYBR/MT quadrant plots were generated using the Attune NxT software v4.2.0
407 (Invitrogen).

408 **Antibody production**

409 Peptides were designed from *P. falciparum* PI3K (PF3D7_0515300) with help from Eurogentec using
410 parameters such as size, amino acid composition, hydrophobicity and secondary structure. Two
411 peptides were chosen - one predicted to be in the catalytic domain and one upstream of this
412 domain, both predicted to be surface-displayed. N-terminal cysteines were added to the peptide
413 sequences to target the coupling site at the carrier protein.
414 Antibodies were raised by Eurogentec. Two rabbits were bled for pre-immune sera, inoculated with
415 both peptides, then further immunised with 3 booster inoculations at 12 days, ~1 month and
416 ~2months. Immune serum was collected after ~9 weeks.

417 **Western blotting**

418 Parasites were extracted from infected erythrocytes by mixing with 0.5 volumes of 0.2% saponin in
419 PBS and incubating for 10 min on ice. Saponin lysates were centrifuged at 15,000 *xg* at 4 °C for 10
420 min, washed 3 x in ice-cold PBS, centrifuged at 15,000 *xg* for 5 min and resuspended in PBS before

421 freezing at -20°C. Parasites obtained by saponin lysis were resuspended in 1x RIPA buffer (150 mM
422 sodium chloride, 1.0% NP-40 or Triton X-100, 0.5% sodium deoxycholate, 0.1% SDS and 50 mM Tris
423 pH 8) with protease inhibitors (ROCHE, cOmplete Mini) added directly before use, then freeze-
424 thawed 3 times. Cell debris was removed by centrifugation at 4 °C, 13,000 *xg*, and supernatant was
425 mixed with 1 x NuPage LDS Sample Buffer (ThermoFisher: NP0007), supplemented with 0.1% 2-
426 mercaptoethanol, then boiled at 90 °C for 5 min. Protein lysates were resolved on 4-15% TRIS-
427 glycine gels (BIO-RAD Mini -PROTEAN® TGX™) for 1–2 h at 100 V in 1X TGS buffer. Wet transfer was
428 completed onto nitrocellulose membrane 0.2-µM-pore-size (Amersham™ Protran®, GE Healthcare)
429 at 60 V for 45 min.

430 Membranes were blocked with 3% BSA TBST for 1 h, washed once in TBST and incubated overnight
431 in primary antibody diluted in blocking buffer at 4 °C. Blots were washed 3x 5 min in TBST and
432 incubated in a secondary antibody diluted 1:5000 in blocking buffer for 1 h. Blots were washed again
433 (3x 5 min, TBST), developed using SuperSignal™ West Pico Plus Chemiluminescent Substrate and
434 imaged on a gel imager (Azure, Q500). Some membranes were stripped prior to re-blocking (10 ml
435 20% SDS and 12.5 ml 0.5M Tris HCL, pH 6.8, added to 77.5 ml distilled water, with 0.8 ml β-
436 mercaptoethanol added just before use). 5 ml stripping buffer (warmed to 50 °C) was added to a
437 blot and incubated at 50 °C for 45 min with agitation. The stripping buffer was removed, and the
438 membrane was washed under a running tap for 1-2 min, then washed 3x 5 min with TBST. The
439 membrane was then ready for re-blocking.

440 Antibodies used were pre-immune or immune sera for *Pf*PI3K peptides, diluted 1:200, with
441 secondary goat anti-rabbit HRP 1:5000 (Abcam, ab97080); or rabbit α-γ-H2aX (Cell signalling, 9718S)
442 with goat α-Rabbit IgG (H+L) Cross-Adsorbed Secondary Antibody, Alexa Fluor™ 594 (Invitrogen, A-
443 11012).

444

445

ACKNOWLEDGEMENTS

We would like to thank Dr Holly Matthews for early work on this project and Profs Marcus Lee and Paul Roepe for helpful discussions.

This work was funded by the European Research Council (ERC) under the European Union's Horizon 2020 research and innovation programme (ERC-2016-COG 725126 to CJM); and a PhD studentship from the University of Cambridge Department of Pathology to MJK. The funders had no role in study design, data collection, interpretation or the decision to submit the work for publication.

REFERENCES

1. WHO. World Malaria Report 2023. 2023. Epub 2023.
2. Klaus S, Binder P, Kim J, Machado M, Funaya C, Schaaf V, et al. Asynchronous nuclear cycles in multinucleated Plasmodium falciparum facilitate rapid proliferation. Sci Adv. 2022;8(13):eabj5362. doi: 10.1126/sciadv.abj5362. PubMed PMID: 35353560.
3. McDonald J, Merrick CJ. DNA replication dynamics during erythrocytic schizogony in the malaria parasites Plasmodium falciparum and Plasmodium knowlesi. PLoS pathogens. 2022;18(6): e1010595.
4. Simon CS, Sturmer VS, Guizetti J. How Many Is Enough? - Challenges of Multinucleated Cell Division in Malaria Parasites. Front Cell Infect Microbiol. 2021;11:658616. doi: 10.3389/fcimb.2021.658616. PubMed PMID: 34026661; PubMed Central PMCID: PMCPMC8137892.
5. Liffner B, Cepeda Diaz AK, Blauwkamp J, Anaguano D, Frolich S, Muralidharan V, et al. Atlas of Plasmodium falciparum intraerythrocytic development using expansion microscopy. Elife. 2023;12. doi: 10.7554/eLife.88088. PubMed PMID: 38108809; PubMed Central PMCID: PMCPMC10727503.
6. Matthews H, Duffy CW, Merrick CJ. Checks and balances? DNA replication and the cell cycle in Plasmodium. Parasit Vectors. 2018;11(1):216. doi: 10.1186/s13071-018-2800-1. PubMed PMID: 29587837; PubMed Central PMCID: PMCPMC5872521.
7. Zhou BB, Elledge SJ. The DNA damage response: putting checkpoints in perspective. Nature. 2000;408(6811):433-9. doi: 10.1038/35044005. PubMed PMID: 11100718.
8. Johnson MK, Chelaghma S, Koreny L, Waller RF, Merrick CJ. Characterisation of cell cycle checkpoint kinases in Toxoplasma gondii. BioRxiv. 2024:doi.org/10.1101/2024.09.10.612042. doi: doi.org/10.1101/2024.09.10.612042;.
9. Lee AH, Symington LS, Fidock DA. DNA repair mechanisms and their biological roles in the malaria parasite Plasmodium falciparum. Microbiol Mol Biol Rev. 2014;78(3):469-86. doi: 10.1128/MMBR.00059-13. PubMed PMID: 25184562; PubMed Central PMCID: PMCPMC4187680.
10. Claessens A, Hamilton WL, Kekre M, Otto TD, Faizullabhoy A, Rayner JC, et al. Generation of antigenic diversity in Plasmodium falciparum by structured rearrangement of Var genes during mitosis. PLoS genetics. 2014;10(12):e1004812. doi: 10.1371/journal.pgen.1004812. PubMed PMID: 25521112; PubMed Central PMCID: PMCPMC4270465.

484 11. Platon L, Menard D. Plasmodium falciparum ring-stage plasticity and drug resistance. Trends
485 Parasitol. 2024;40(2):118-30. doi: 10.1016/j.pt.2023.11.007. PubMed PMID: 38104024.
486 12. Gupta DK, Patra AT, Zhu L, Gupta AP, Bozdech Z. DNA damage regulation and its role in drug-
487 related phenotypes in the malaria parasites. Sci Rep. 2016;6:23603. doi: 10.1038/srep23603.
488 PubMed PMID: 27033103; PubMed Central PMCID: PMCPMC4817041.
489 13. Absalon S, Dvorin JD. Depletion of the mini-chromosome maintenance complex binding
490 protein allows the progression of cytokinesis despite abnormal karyokinesis during the asexual
491 development of Plasmodium falciparum. Cellular microbiology. 2021;23(3):e13284. doi:
492 10.1111/cmi.13284. PubMed PMID: 33124706; PubMed Central PMCID: PMCPMC8058698.
493 14. Janse CJ, van der Klooster PF, van der Kaay HJ, van der Ploeg M, Overdulve JP. DNA synthesis
494 in Plasmodium berghei during asexual and sexual development. Molecular and biochemical
495 parasitology. 1986;20(2):173-82. doi: 10.1016/0166-6851(86)90029-0. PubMed PMID: 3092048.
496 15. Matthews H, McDonald J, Totanes FIG, Merrick CJ. Dynamics of DNA replication during male
497 gametogenesis in the malaria parasite Plasmodium falciparum. Cellular microbiology. 2022. doi:
498 doi.org/10.1101/2021.12.18.473304
499 16. Merrick CJ, Jackson D, Diffley JF. Visualization of altered replication dynamics after DNA
500 damage in human cells. The Journal of biological chemistry. 2004;279(19):20067-75. PubMed PMID:
501 14982920.
502 17. Santocanale C, Diffley JF. A Mec1- and Rad53-dependent checkpoint controls late-firing
503 origins of DNA replication. Nature. 1998;395(6702):615-8. doi: 10.1038/27001. PubMed PMID:
504 9783589.
505 18. Goyal M, Heinberg A, Mitesser V, Kandelis-Shalev S, Singh BK, Dzikowski R. Phosphorylation
506 of the Canonical Histone H2A Marks Foci of Damaged DNA in Malaria Parasites. mSphere. 2021;6(1).
507 doi: 10.1128/mSphere.01131-20. PubMed PMID: 33441412; PubMed Central PMCID:
508 PMCPMC7845613.
509 19. Helt CE, Cliby WA, Keng PC, Bambara RA, O'Reilly MA. Ataxia telangiectasia mutated (ATM)
510 and ATM and Rad3-related protein exhibit selective target specificities in response to different forms
511 of DNA damage. The Journal of biological chemistry. 2005;280(2):1186-92. doi:
512 10.1074/jbc.M410873200. PubMed PMID: 15533933.
513 20. Rogakou EP, Pilch DR, Orr AH, Ivanova VS, Bonner WM. DNA double-stranded breaks induce
514 histone H2AX phosphorylation on serine 139. The Journal of biological chemistry.
515 1998;273(10):5858-68. doi: 10.1074/jbc.273.10.5858. PubMed PMID: 9488723.
516 21. Beranek DT. Distribution of methyl and ethyl adducts following alkylation with
517 monofunctional alkylating agents. Mutat Res. 1990;231(1):11-30. doi: 10.1016/0027-5107(90)90173-
518 2. PubMed PMID: 2195323.
519 22. Gopalakrishnan AM, Kumar N. Opposing roles for two molecular forms of replication protein
520 A in Rad51-Rad54-mediated DNA recombination in Plasmodium falciparum. mBio.
521 2013;4(3):e00252-13. doi: 10.1128/mBio.00252-13. PubMed PMID: 23631919; PubMed Central
522 PMCID: PMCPMC3648904.
523 23. Craven HM, Nettesheim G, Cicuta P, Blagborough AM, Merrick CJ. Effects of the G-
524 quadruplex-binding drugs quarfloxin and CX-5461 on the malaria parasite Plasmodium falciparum.
525 Int J Parasitol Drugs Drug Resist. 2023;23:106-19. doi: 10.1016/j.ijpddr.2023.11.007. PubMed PMID:
526 38041930; PubMed Central PMCID: PMCPMC10711401.
527 24. Mbengue A, Bhattacharjee S, Pandharkar T, Liu H, Estiu G, Stahelin RV, et al. A molecular
528 mechanism of artemisinin resistance in Plasmodium falciparum malaria. Nature.
529 2015;520(7549):683-7. doi: 10.1038/nature14412. PubMed PMID: 25874676; PubMed Central
530 PMCID: PMCPMC4417027.
531 25. Hassett MR, Roepe PD. PIK-ing New Malaria Chemotherapy. Trends Parasitol.
532 2018;34(11):925-7. doi: 10.1016/j.pt.2018.06.003. PubMed PMID: 29934102.

533 26. Hassett MR, Sternberg AR, Riegel BE, Thomas CJ, Roepe PD. Heterologous Expression,
534 Purification, and Functional Analysis of Plasmodium falciparum Phosphatidylinositol 3'-Kinase.
535 Biochemistry. 2017;56(33):4335-45. doi: 10.1021/acs.biochem.7b00416. PubMed PMID: 28719180.
536 27. Tawk L, Chicanne G, Dubremetz JF, Richard V, Payrastre B, Vial HJ, et al. Phosphatidylinositol
537 3-phosphate, an essential lipid in Plasmodium, localizes to the food vacuole membrane and the
538 apicoplast. Eukaryotic cell. 2010;9(10):1519-30. doi: 10.1128/EC.00124-10. PubMed PMID:
539 20709789; PubMed Central PMCID: PMCPMC2950420.
540 28. Vaid A, Ranjan R, Smythe WA, Hoppe HC, Sharma P. PfPI3K, a phosphatidylinositol-3 kinase
541 from Plasmodium falciparum, is exported to the host erythrocyte and is involved in hemoglobin
542 trafficking. Blood. 2010;115(12):2500-7. doi: 10.1182/blood-2009-08-238972. PubMed PMID:
543 20093402; PubMed Central PMCID: PMCPMC2918364.
544 29. Thomas D, Powell JA, Green BD, Barry EF, Ma Y, Woodcock J, et al. Protein kinase activity of
545 phosphoinositide 3-kinase regulates cytokine-dependent cell survival. PLoS biology.
546 2013;11(3):e1001515. doi: 10.1371/journal.pbio.1001515. PubMed PMID: 23526884; PubMed
547 Central PMCID: PMCPMC3601961.
548 30. Foukas LC, Shepherd PR. Phosphoinositide 3-kinase: the protein kinase that time forgot.
549 Biochem Soc Trans. 2004;32(Pt 2):330-1. doi: 10.1042/bst0320330. PubMed PMID: 15046601.
550 31. Reaper PM, Griffiths MR, Long JM, Charrier JD, Maccormick S, Charlton PA, et al. Selective
551 killing of ATM- or p53-deficient cancer cells through inhibition of ATR. Nat Chem Biol. 2011;7(7):428-
552 30. doi: 10.1038/nchembio.573. PubMed PMID: 21490603.
553 32. Hickson I, Zhao Y, Richardson CJ, Green SJ, Martin NM, Orr AI, et al. Identification and
554 characterization of a novel and specific inhibitor of the ataxia-telangiectasia mutated kinase ATM.
555 Cancer research. 2004;64(24):9152-9. doi: 10.1158/0008-5472.CAN-04-2727. PubMed PMID:
556 15604286.
557 33. Ismail HM, Barton V, Phanchana M, Charoensutthivarakul S, Wong MH, Hemingway J, et al.
558 Artemisinin activity-based probes identify multiple molecular targets within the asexual stage of the
559 malaria parasites Plasmodium falciparum 3D7. Proceedings of the National Academy of Sciences of
560 the United States of America. 2016;113(8):2080-5. doi: 10.1073/pnas.1600459113. PubMed PMID:
561 26858419; PubMed Central PMCID: PMCPMC4776496.
562 34. Xiong A, Prakash P, Gao X, Chew M, Tay IJJ, Woodrow CJ, et al. K13-Mediated Reduced
563 Susceptibility to Artemisinin in Plasmodium falciparum Is Overlaid on a Trait of Enhanced DNA
564 Damage Repair. Cell Rep. 2020;32(5):107996. doi: 10.1016/j.celrep.2020.107996. PubMed PMID:
565 32755588; PubMed Central PMCID: PMCPMC7408483.
566 35. Gopalakrishnan AM, Kumar N. Antimalarial action of artesunate involves DNA damage
567 mediated by reactive oxygen species. Antimicrobial agents and chemotherapy. 2015;59(1):317-25.
568 doi: 10.1128/AAC.03663-14. PubMed PMID: 25348537; PubMed Central PMCID: PMCPMC4291367.
569 36. Straimer J, Gnadig NF, Witkowski B, Amaratunga C, Duru V, Ramadani AP, et al. Drug
570 resistance. K13-propeller mutations confer artemisinin resistance in Plasmodium falciparum clinical
571 isolates. Science (New York, NY. 2015;347(6220):428-31. doi: 10.1126/science.1260867. PubMed
572 PMID: 25502314; PubMed Central PMCID: PMCPMC4349400.
573 37. Davis SZ, Singh PP, Vendrely KM, Shoue DA, Checkley LA, McDew-White M, et al. The
574 extended recovery ring-stage survival assay provides a superior association with patient clearance
575 half-life and increases throughput. Malaria journal. 2020;19(1):54. doi: 10.1186/s12936-020-3139-6.
576 PubMed PMID: 32005233; PubMed Central PMCID: PMCPMC6995136.
577 38. Merrick CJ. Transfection with thymidine kinase permits bromodeoxyuridine labelling of DNA
578 replication in the human malaria parasite Plasmodium falciparum. Malar J. 2015;14(490). doi:
579 10.1186/s12936-015-1014-7.
580 39. Courtot L, Hoffmann JS, Bergoglio V. The Protective Role of Dormant Origins in Response to
581 Replicative Stress. Int J Mol Sci. 2018;19(11). doi: 10.3390/ijms19113569. PubMed PMID: 30424570;
582 PubMed Central PMCID: PMCPMC6274952.

583 40. Mott BT, Eastman RT, Guha R, Sherlach KS, Siriwardana A, Shinn P, et al. High-throughput
584 matrix screening identifies synergistic and antagonistic antimalarial drug combinations. Sci Rep.
585 2015;5:13891. doi: 10.1038/srep13891. PubMed PMID: 26403635; PubMed Central PMCID:
586 PMCPMC4585899.
587 41. Totanes FIG, Gockel J, Chapman SE, Bartfai R, Boemo MA, Merrick CJ. A genome-wide map
588 of DNA replication at single-molecule resolution in the malaria parasite Plasmodium falciparum.
589 Nucleic acids research. 2023. doi: 10.1093/nar/gkad093. PubMed PMID: 36808528.
590 42. Smilkstein M, Sriwilaijaroen N, Kelly JX, Wilairat P, Riscoe M. Simple and inexpensive
591 fluorescence-based technique for high-throughput antimalarial drug screening. Antimicrobial agents
592 and chemotherapy. 2004;48(5):1803-6. PubMed PMID: 15105138; PubMed Central PMCID:
593 PMCPMC400546.
594 43. Huang RY, Pei L, Liu Q, Chen S, Dou H, Shu G, et al. Isobologram Analysis: A Comprehensive
595 Review of Methodology and Current Research. Front Pharmacol. 2019;10:1222. doi:
596 10.3389/fphar.2019.01222. PubMed PMID: 31736746; PubMed Central PMCID: PMCPMC6830115.
597 44. Fivelman QL, Adagu IS, Warhurst DC. Modified fixed-ratio isobologram method for studying
598 in vitro interactions between atovaquone and proguanil or dihydroartemisinin against drug-resistant
599 strains of Plasmodium falciparum. Antimicrobial agents and chemotherapy. 2004;48(11):4097-102.
600 doi: 10.1128/AAC.48.11.4097-4102.2004. PubMed PMID: 15504827; PubMed Central PMCID:
601 PMCPMC525430.
602 45. Safeukui I, Ware RE, Mohandas N, Haldar K. Simultaneous adjunctive treatment of malaria
603 and its coevolved genetic disorder sickle cell anemia. Blood Adv. 2023;7(19):5970-81. doi:
604 10.1182/bloodadvances.2022009124. PubMed PMID: 37093647; PubMed Central PMCID:
605 PMCPMC10580175 interests.
606 46. Yang J, Yan R, Roy A, Xu D, Poisson J, Zhang Y. The I-TASSER Suite: protein structure and
607 function prediction. Nature methods. 2015;12(1):7-8. doi: 10.1038/nmeth.3213. PubMed PMID:
608 25549265; PubMed Central PMCID: PMCPMC4428668.

609

610 **FIGURE LEGENDS**

611 Figure 1: Evidence for DNA-damage-responsive checkpoint activity in *P. falciparum*

612 A. BrdU incorporation into populations of trophozoites at three stages, after treatment with
613 MMS, as measured by ELISA. Parasites were treated with MMS for 1 h and BrdU was added
614 for the latter 30 mins. Means of two biological replicates, conducted in technical triplicate,
615 are shown; error bars show range. MMS treatments: 10x IC_{50}, 960 µM; 20x IC_{50}, 1.92 mM.
616 For each parasite stage, statistical testing was via ordinary one-way ANOVA and posthoc
617 Tukey's multiple comparisons test. *, P-value <0.05; comparisons not shown, ns. Pictures
618 show examples of trophozoites at each timepoint. Scale bar, 2µm.
619 B. Representative western blot of phosphorylated histone in trophozoite parasite lysate
620 treated with MMS (2 h, 10x IC_{50}). Phosphorylated histone signal was quantified versus

621 control histone H4: relative quantification is shown below the blot. Graph shows
622 quantifications from three biological replicate blots, relative to either H4 or Hsp70 as a
623 control protein. Unpaired two-tailed t-test: P-value = 0.0354.
624
625 Figure 2: *Pf*PI3K does not visibly relocate to the nucleus upon DNA damage

626 A. Western blots showing detection of *Pf*PI3K by two antisera raised to *Pf*PI3K peptides.
627 Replicate lanes from the same blot of protein lysate from late-stage *P. falciparum* were
628 exposed to either pre-immune or immune serum. Histone H4 was used as a loading control.
629 B. Immunofluorescence assay (IFA) showing location of *Pf*PI3K (detected by antiserum 1) in *P.*
630 *falciparum*. 2-3 representative cells are shown per stage. Scale bar 1 µm.
631 C. IFA showing *Pf*PI3K in *P. falciparum* after DNA damage: 1 h treatment with 5x or 10x IC_{50} of
632 DHA or MMS on late-stage parasites. One representative cell per condition is shown. Scale
633 bar 1µm.
634

635 Figure 3: Inhibitors of human PIKKs synergise with the DNA-damaging agent MMS in *P. falciparum*

636 A. Inhibition of parasite growth by VE-821 and KU-55933 (molecular structures of each
637 inhibitor are shown). Growth curves from five independent malaria SYBR green I-based
638 fluorescence (MSF) assays: percentage parasite growth is plotted as a function of drug
639 concentration, error bars are standard errors of the means. Mean IC_{50}s from all experiments
640 are shown (individual IC_{50} values from replicate experiments are in Fig S1B).
641 B. Isobolograms plotted as fractional inhibitory concentrations (FIC) of combinations of MMS
642 and VE-821 or KU-55933, as determined by MSF assay. FIC calculations were completed for
643 each combination by dividing the measured "apparent" IC_{50} values for individual drugs in the
644 different combinations by IC_{50} values obtained when the drugs were used alone. Each curve
645 represents a different biological replicate experiment. The mean FIC ($\Sigma FIC(FIC_A+FIC_B)$) is

646 shown, with range. The type of relationship was defined as moderately synergistic based on
647 well-established criteria: ∑FIC <0.5, substantial synergism; ∑FIC <1, moderate synergism;
648 ∑FIC ≥1 and <2, additive interaction; ∑FIC ≥2 and <4, slight antagonism and ∑FIC >4, marked
649 antagonism [45].

650 C. BrdU incorporation into 30-32 hpi trophozoites after treatment with MMS, VE-821, KU-
651 55933, geneticin and combinations of these, measured by ELISA. Parasites were treated with
652 10x IC_{50} of drug for 1 h and BrdU was added for the latter 30 mins. Six biological replicates
653 are plotted, each completed in technical triplicate. Mean and standard deviation error bars
654 are plotted, values normalised to control (set to 100%) in each replicate. Concentrations of
655 drugs used: MMS 960 μM, VE-821 1.62 μM, KU-55933 400 μM, geneticin 1500 μg/ml.
656 Ordinary one-way ANOVA and posthoc Tukey's multiple comparisons test of control vs all
657 and MMS vs all was completed; P-values: *, <0.05; **, <0.01; ***, <0.001; ****, <0.0001;
658 comparisons not shown, ns.

659

660 Figure 4: The antimalarial drug dihydroartemisinin induces a DNA replication arrest in *P. falciparum*

661 A. BrdU incorporation into 30-32 hpi trophozoites after treatment with DHA, VE-821, KU-55933
662 and combination treatments. Parasites were treated with 10X IC_{50} of drug for 1 h and BrdU
663 was added for the latter 30 mins. Five biological replicates were plotted, each completed in
664 technical triplicate. Mean and standard deviation error bars are plotted; values were
665 normalised to control (set to 100%) in each replicate. Concentrations of drugs used: DHA 45
666 nM, VE-821 1.62 μM, KU-55933 400 μM. Statistical testing by ordinary one-way ANOVA and
667 posthoc Tukey's multiple comparisons test of control vs all and DHA vs all; P-values: *, <0.05;
668 comparisons not shown, ns.

669 B. Isobolograms plotted as Figure 4B. Each curve is a biological replicate and the mean FIC
670 ($\Sigma FIC(FIC_A+FIC_B)$) is shown, with range. The relationship between DHA and either VE-821 or
671 KU55933 was defined as additive.
672
673 Figure 5: Ring-stage survival is affected by PIKK inhibitors

674 Data in A-D are from eRRSA assays on the strains 3D7, MRA-1252 and MRA-1240. Samples were
675 treated with DMSO (the control condition), VE-821, KU-55933, DHA and combinations of these. Drug
676 concentrations: VE-821, 81 nM (0.5X IC_{50}); KU-55933, 20 μM (0.5X IC_{50}); DMSO, 0.02%; DHA, 700 nM.
677 Values plotted are the means of -log(foldchange = 2^(DHA-DMSO)) for each treatment. Midline
678 represents the mean and boxes show min to max from three biological replicates, each conducted in
679 technical triplicate. Statistical testing by ordinary one-way ANOVA and Dunnett's multiple
680 comparisons test, comparing all means to the mean value from DMSO- or DHA-treated samples. P-
681 values: *, <0.05; **, <0.01; ***, <0.001; ****, <0.0001. Differences between DHA-treated samples
682 and treatments other than the control did not reach statistical significance.
683 A. Ring-stage DHA-sensitive parasite strains, 3D7 or MRA-1252, were treated with DMSO (control
684 condition), DHA and inhibitors VE-821 or KU-55933 in combination with DHA for a 6 h pulse, then
685 left to recover for 72 h.
686 B. Control experiments without DHA: ring-stage 3D7 or MRA-1252 parasites were treated with
687 DMSO or inhibitors VE-821 or KU-55933 for a 6 h pulse, then left to recover for 72 h.
688 C. Ring-stages of the DHA-resistant parasite strain MRA-1240 were treated with DMSO (control
689 condition), DHA and inhibitors VE-821 or KU-55933 in combination with DHA for a 6 h pulse, then
690 left to recover for 72 h.
691 D. Control experiment without DHA: ring-stage MRA-1240 parasites were treated with DMSO or
692 inhibitors VE-821 or KU-55933 for a 6 h pulse, then left to recover for 72 h.
693 E. Inhibition of growth over a full 48h growth cycle by MMS, VE-821 and KU55933 was measured in
694 the strains 3D7, MRA-1252 and MRA-1240 via MSF assay. IC_{50}s were calculated from at least

695 three independent experiments and all values are plotted, with the midline showing the mean
696 and error bars showing standard deviation. MSF growth curves are in Fig S1C.
697

698 **SUPPLEMENTARY FIGURE LEGENDS**

699 Figure S1: Growth curves determining IC_{50} values for MMS, VE-821 and KU-55933 in the parasite
700 strains 3D7, MRA-1252 and MRC-1240.

701 Each panel shows growth curves from 3-5 independent malaria SYBR green I-based
702 fluorescence (MSF) assays: percentage parasite growth is plotted as a function of drug
703 concentration; error bars are standard errors of the means.
704 A. Inhibition of growth of 3D7 strain by MMS.
705 B. IC_{50} values from the growth curves shown in main figure 3A.
706 C. Inhibition of strains MRA-1252 and MRA-1240 by the drugs VE-821, KU55933 and MMS.
707

708 Figure S2: 3D7 parasites survive a short pulse of MMS or DHA at the trophozoite stage, but their
709 maturation is delayed and progeny number per schizont, reduced.

710 A. Images were taken 12h after trophozoites at 30-32hpi had been exposed to a 1 h pulse of
711 10X IC_{50} MMS or DHA (2 independent experiments, '1' and '2'). Images show that at this
712 timepoint (i.e. 42-44hpi), cultures were dominated by a mixture of immature and mature
713 schizonts, without clear evidence of parasite death in the damaged cultures. Parasites were
714 then treated with 75nM ML10 for 10 h, to arrest mature schizonts before egress, and re-
715 imaged. Mature schizonts then dominated in all cultures.
716 B. Parasite stages imaged in (A) were categorised as either: early rings, small rings, large rings,
717 early trophozoites, mid trophozoites, late trophozoites, immature schizonts or mature
718 schizonts (2 independent experiments, $n \geq 100$ from each experiment). Differences between
719 the proportions of stages in control vs DHA-treated vs MMS-treated cultures were tested via

720 two-way ANOVA and posthoc Tukey's multiple comparisons test. P-values are shown in a
721 table below the graph: *, <0.05; **, <0.01; ***, <0.001. Stars of matched colours across
722 rows denote a significant difference between those conditions (e.g. at 44hpi, there were still
723 more immature schizonts after MMS treatment than in the control (pink stars); 10h later,
724 this difference disappeared, with more mature and fewer immature schizonts (denoted by
725 pairs of yellow and blue stars). The only other difference was in the small numbers of rings
726 that escaped and reinvaded after prolonged arrest.

727 C. Merozoites per schizont were counted in each of the cultures shown in (A) (n = 26-30 per
728 culture). Numbers of merozoites substantially increased in all cultures after the long ML10-
729 arrest period, which allowed mature schizonts to accumulate even after the damage-
730 induced delay seen in (B). A reduction in merozoite number was, however, still seen after
731 MMS damage, although this was not significant after DHA damage.

732

733 Figure S3: Protein sequence alignment of *P. falciparum* PI3K, PI4K and PIKKs from *S. cerevisiae* and
734 human.

735 MUSCLE (3.8) alignment of catalytic domains of *P. falciparum* PI3K and PI4K against human ATM,
736 ATR, PI3K, and yeast Mec1 and Tel1. Colour key is ClustalW standard. Highlighted in the yellow boxes
737 are the catalytic loops in ATR and ATM. Percentage identity matrix is shown below the alignment.

738

739 Figure S4: Anti-*Pf*PI3K antibody production

740 A. Model made in i-TASSER [46], threading 1500 C-terminal residues of the 2133-amino acid
741 *Pf*PI3K against human ATR. Protein coloured blue to red, N-terminal to C-terminal. Peptides
742 used as antigens are highlighted in white and circled: amino acids 1359-1374 and 2011-2025
743 of full length *Pf*PI3K.

744 B. Controls for specificity of immune versus pre-immune antisera against *Pf*PI3K.

745 Representative images of single cells are shown. Scale bar 1 µm. Primary antibodies used

746 were rabbit antisera, pre-immune or immune, diluted 1:200 in 3% BSA.

747

748 Figure S5: Isobolograms showing that two antibiotic drugs do not synergise with MMS

749 Isobolograms plotted as fractional inhibitory concentrations (FIC) of combinations of MMS and

750 geneticin (G-418), or blasticidin (BSD), as determined by MSF assay. Data were processed as in

751 Figure 4B. The type of relationship was defined as additive for blasticidin and borderline

752 antagonistic for geneticin, based on well-established criteria (∑FIC <0.5, substantial synergism;

753 ∑FIC <1, moderate synergism; ∑FIC ≥1 and <2, additive interaction; ∑FIC ≥2 and <4, slight

754 antagonism and ∑FIC >4, marked antagonism).

755

756 Figure S6: Ring stage survival assessed by flow cytometry

757 A ring-stage survival assay was assessed by flow cytometry as well as eRRSA as used in Figure 5.

758 Density plot quadrant graphs show one biological replicate of an RSA conducted on 3D7. Cell counts

759 for each quadrant are shown. Percentage survival was calculated as the proportion of live versus

760 dead cells (SYBR+ MITO+/SYBR+ MITO-) for each condition.

761

Figure 1:

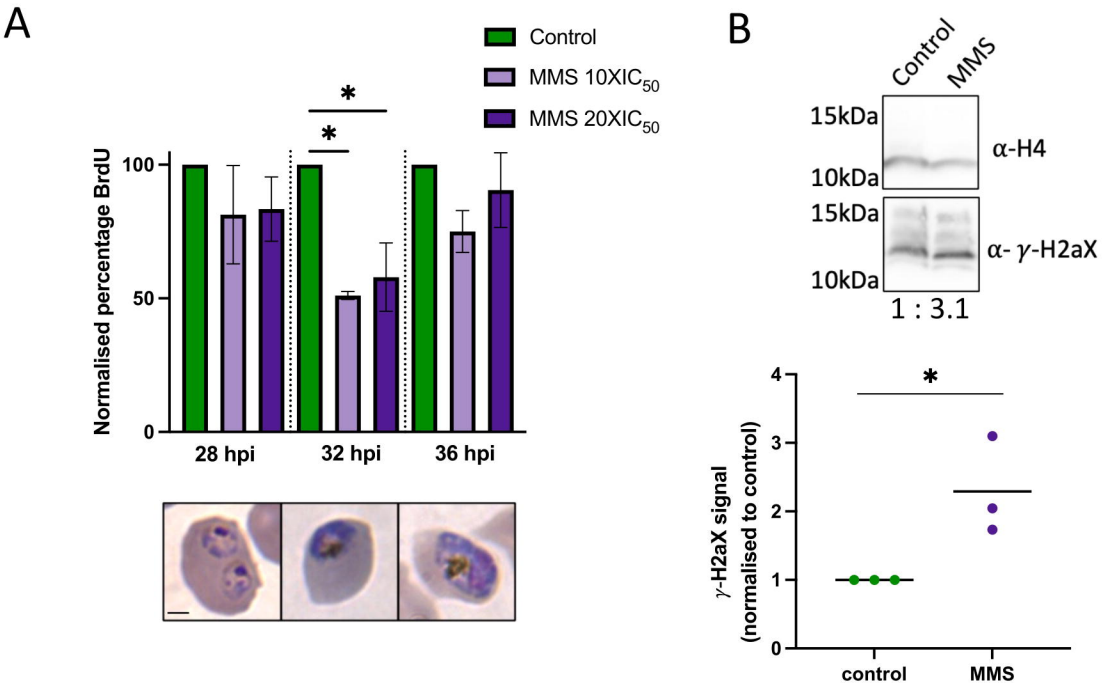
A
Control
MMS 10XIC50
MMS 20XIC50
*
*
Normalised percentage BrdU
100
50
0
28 hpi
32 hpi
36 hpi
B
Control
MMS
15kDa
10kDa
α-H4
15kDa
10kDa
α- γ-H2aX
1 : 3.1
*
γ-H2aX signal
(normalised to control)
4
3
2
1
0
control
MMS

Figure 2:

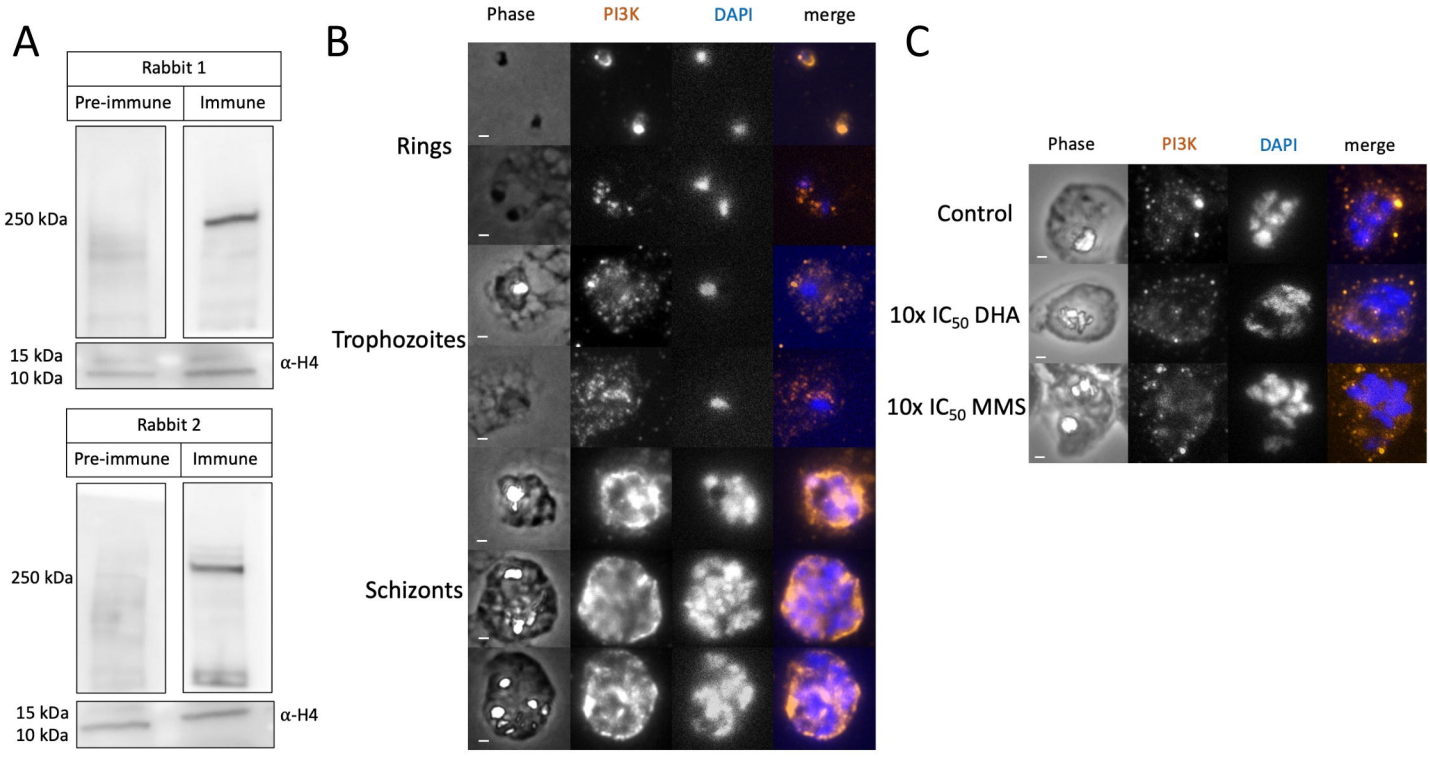
A
Rabbit 1
Pre-immune
Immune
250 kDa
15 kDa
10 kDa
α-H4
Rabbit 2
Pre-immune
Immune
250 kDa
15 kDa
10 kDa
α-H4
B
Phase
PI3K
DAPI
merge
Rings
Trophozoites
Schizonts
C
Phase
PI3K
DAPI
merge
Control
10x IC50 DHA
10x IC50 MMS

Figure 3:

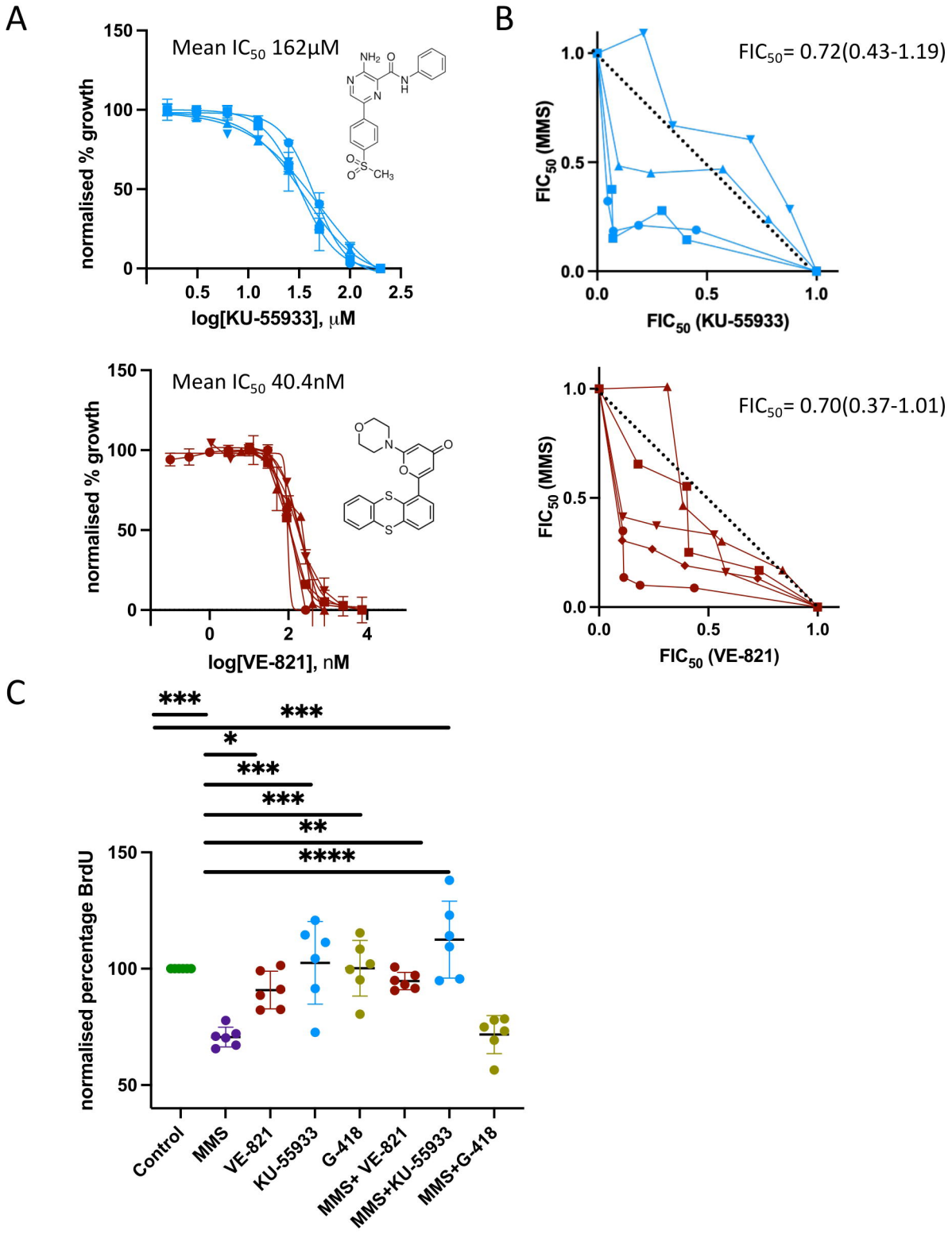
A
Mean IC50 162μM
normalised % growth
log[KU-55933], μM
Mean IC50 40.4nM
log[VE-821], nM
B
FIC50= 0.72(0.43-1.19)
FIC50 (MMS)
FIC50 (KU-55933)
FIC50= 0.70(0.37-1.01)
FIC50 (VE-821)
C
normalised percentage BrdU
Control
MMS
VE-821
KU-55933
G-418
MMS+ VE-821
MMS+KU-55933
MMS+G-418

Figure 4:

A

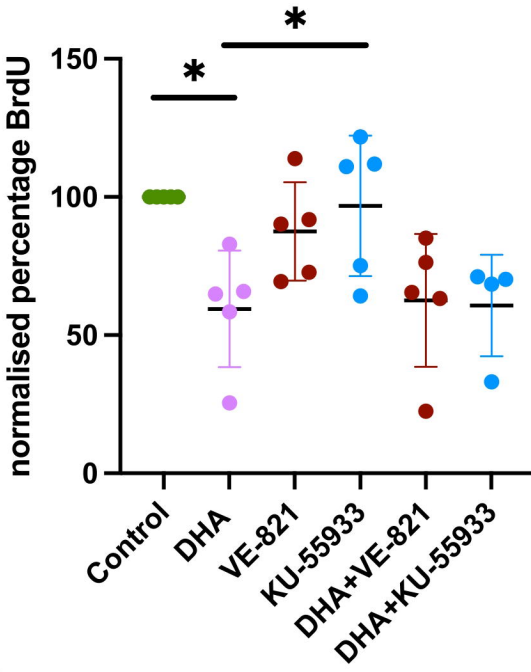
*
*
150
100
50
0
normalised percentage BrdU
Control
DHA
VE-821
KU-55933
DHA+VE-821
DHA+KU-55933

B

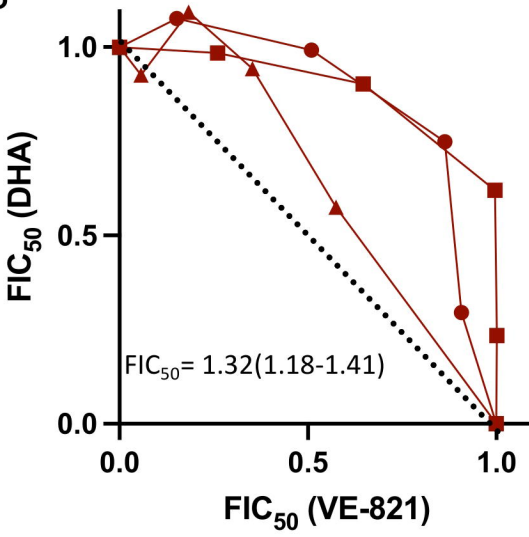
1.0
0.5
0.0
FIC50 (DHA)
FIC50= 1.32(1.18-1.41)
0.0
0.5
1.0
FIC50 (VE-821)

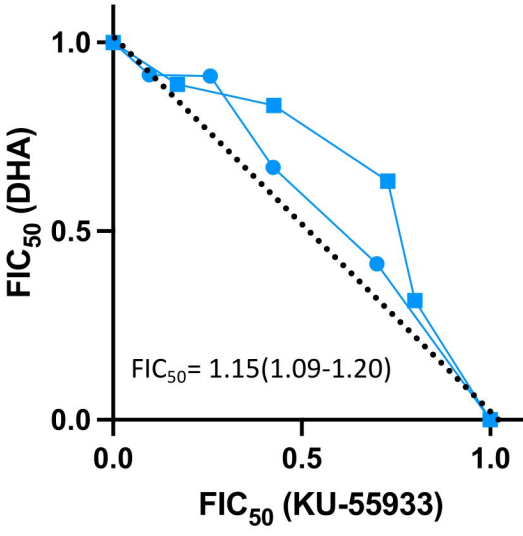
1.0
0.5
0.0
FIC50 (DHA)
FIC50= 1.15(1.09-1.20)
0.0
0.5
1.0
FIC50 (KU-55933)

Figure 5:

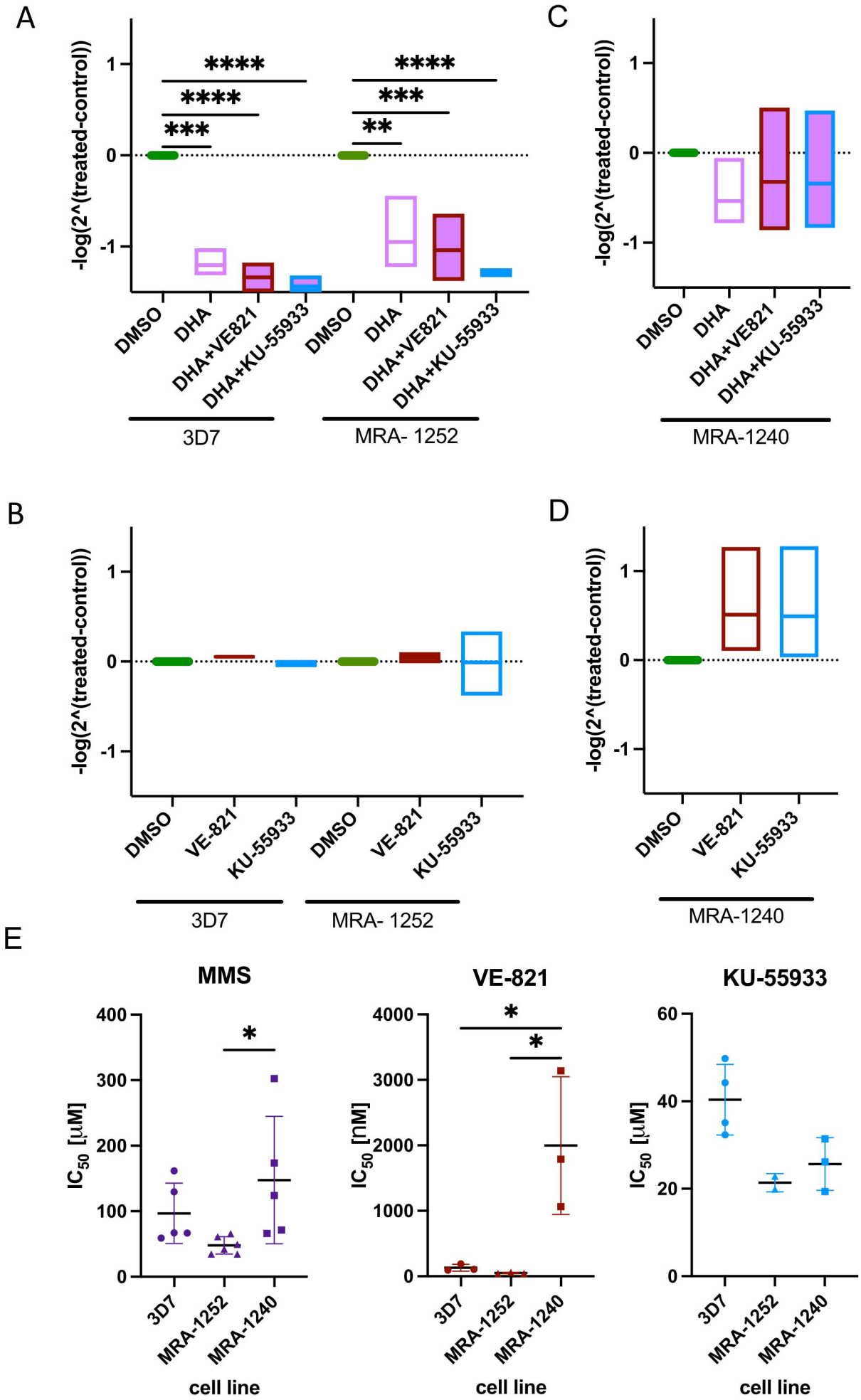
A
-log(2^(treated-control))
1
0
-1
****
****
***
****
***
**
DMSO
DHA
DHA+VE821
DHA+KU-55933
DMSO
DHA
DHA+VE821
DHA+KU-55933
3D7
MRA- 1252
C
-log(2^(treated-control))
1
0
-1
DMSO
DHA
DHA+VE821
DHA+KU-55933
MRA-1240
B
-log(2^(treated-control))
1
0
-1
DMSO
VE-821
KU-55933
DMSO
VE-821
KU-55933
3D7
MRA- 1252
D
-log(2^(treated-control))
1
0
-1
DMSO
VE-821
KU-55933
MRA-1240
E
MMS
VE-821
KU-55933
IC50 [µM]
400
300
200
100
0
*
IC50 [nM]
4000
3000
2000
1000
0
*
*
IC50 [µM]
60
40
20
0
3D7
MRA-1252
MRA-1240
cell line